Research article **Open Access**

Evangelos Atmatzakis, Nikitas Papasimakis*, Vassili Fedotov, Guillaume Vienne and Nikolay I. Zheludev

Magneto-optical response in bimetallic metamaterials

DOI 10.1515/nanoph-2016-0162
Received September 22, 2016; revised November 30, 2016; accepted December 7, 2016

Abstract: We demonstrate resonant Faraday polarization rotation in plasmonic arrays of bimetallic nano-ring resonators consisting of Au and Ni sections. This metamaterial design allows the optimization of the trade-off between the enhancement of magneto-optical effects and plasmonic dissipation. Nickel sections corresponding to as little as ~6% of the total surface of the metamaterial result in magneto-optically induced polarization rotation equal to that of a continuous nickel film. Such bimetallic metamaterials can be used in compact magnetic sensors, active plasmonic components, and integrated photonic circuits.

Keywords: magnetoplasmonics; metamaterials; metasurfaces; bimetallic; Faraday rotation.

1 Introduction

The ability to tailor light-matter interactions is equally important for the development of current and future technologies (telecommunications, sensing, data storage), as well as for the study of the fundamental properties of matter (spectroscopy). A typical example involves the exploitation of magneto-optical (MO) effects, where quasistatic magnetic fields can induce optical anisotropy in a material. This is a direct manifestation of the Zeeman effect, the splitting of electronic energy levels due to interactions between magnetic fields and the magnetic dipole moment associated with the orbital and spin angular momentum [1]. This energy splitting gives rise to numerous polarization phenomena, such as magnetically induced birefringence and dichroism, which enable dynamic control over the polarization state of light.

In recent years, magnetoplasmonics, the study of systems that combine plasmonic and magnetic properties of matter, holds promise to both enhance MO effects and to enable non-reciprocal, magnetic-field-controlled plasmonic devices [2–7]. Ferromagnetic metals, such as Fe, Ni, and Co, are known to be magneto-optically active but have poor plasmonic properties in the near-infrared (NIR) spectral range due to high Joule losses. In contrast, noble metals suffer less from loss, but exhibit negligible MO response. Hence, by combining ferromagnetic and noble metals, one can construct a system with strong MO response. Indeed, early studies identified dramatic enhancement of the MO response due to strongly localized electromagnetic fields associated with plasmonic resonances. In particular, enhanced Faraday effect (FE) and magneto-optical Kerr effect (MOKE) have been observed in hybrid devices that simultaneously support plasmonic resonances and are MO active [8–10]. Furthermore, nanostructuring of magnetoplasmonic systems provides control over the frequency dispersion and phase of MO effects [3, 6, 7, 11–14] while maintaining a compact form factor. In bulk homogeneous media, strong MO effects require long interaction lengths between light and matter. However, the light confinement originating from nanostructuring can offer similar response at significantly smaller dimensions, an often required property for the realization of compact modulators, isolators, and circulators [15]. On the other hand, the presence of external magnetic fields can be employed to control the plasmonic response, a desirable functionality in sensing applications [16, 17].

***Corresponding author: Nikitas Papasimakis,** Optoelectronics Research Centre and Centre for Photonic Metamaterials, University of Southampton, Southampton SO17 1BJ, UK, e-mail: n.papasimakis@soton.ac.uk
Evangelos Atmatzakis and Vassili Fedotov: Optoelectronics Research Centre and Centre for Photonic Metamaterials, University of Southampton, Southampton SO17 1BJ, UK
Guillaume Vienne: Data Storage Institute, Agency for Science, Technology and Research (A*STAR), Singapore 117608, Singapore; and School of Electrical and Electronic Engineering, Nanyang Technological University, Singapore 639798, Singapore
Nikolay I. Zheludev: Optoelectronics Research Centre and Centre for Photonic Metamaterials, University of Southampton, Southampton SO17 1BJ, UK; and The Photonics Institute and Centre for Disruptive Photonic Technologies, Nanyang Technological University, Singapore 637371, Singapore

Magnetoplasmonic metamaterials, consisting of arrays of plasmonic resonators hybridized with MO materials, employ resonant plasmonic fields to maximize the enhancement of MO effects. The MO active material can be introduced either as substrate/superstrate or as part of the plasmonic resonator. Since the enhancement of MO effects occurs mainly where the resonant plasmonic fields overlap with the MO active components, very compact magnetoplasmonic devices can be realized. Here, we implement for the first time a design for magnetoplasmonic metamaterials, where the MO active component is integrated directly into the plasmonic resonators. The MO response is provided by a small Ni section, which is combined with a gold split-ring to form a bimetallic ring resonator (as illustrated in Figure 1A). This design allows the optimization of the trade-off between dissipation loss (which weakens the plasmonic fields) and the strength of the MO response. In particular, by increasing the size of the Ni section, dissipation loss increases due to the presence of a larger (lossy) Ni section. At the same time, the strength of the MO response is expected to increase, as the Ni sector also provides the MO response. Varying the composition of the ring allows one to maximize the strength of magnetoplasmonic response of the system. Moreover, changing the wavelength or polarization of the incident light allows one to shift the area of light confinement along the resonator and thus control the MO response. Finally, our approach is based on continuous metallic nanostructures and enables not only to realize complex resonators with prescribed MO and plasmonic response but also to exploit other types of physical response involving thermal and electric effects [18, 19].

2 Results and discussion

A strong plasmonic resonance can be excited in a bimetallic metamaterial array under illumination with light polarized in the plane of symmetry of the resonators (yz plane – see Figure 1A). The characteristic case of a metamaterial with a 90° Ni sector is presented in Figure 1B, where the resonance is seen as a transmission dip at a wavelength of ~850 nm. The experimental transmission spectrum (solid red line) is in good agreement with the results of numerical modeling (dashed red line). At the resonance, the electric field profile exhibits two "hot spots" of charge concentration with currents oscillating in-phase between the hot spots (see inset to Figure 1B). This symmetric current configuration corresponds to the lowest order

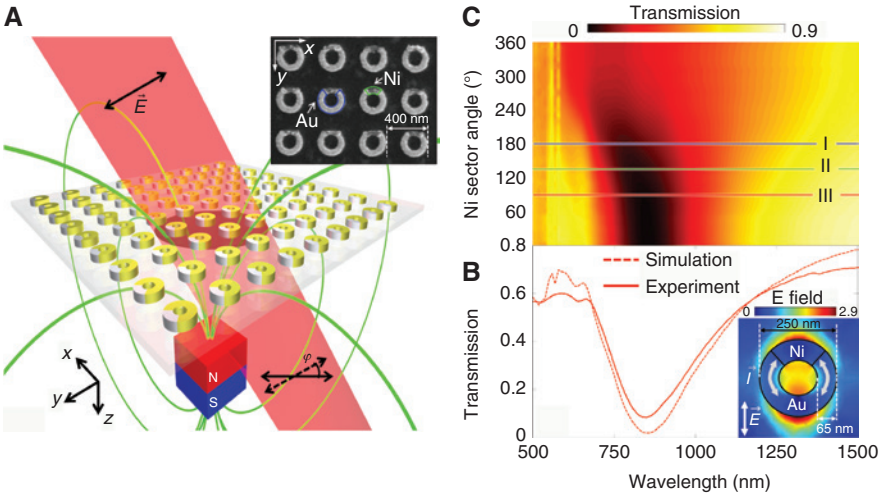

Figure 1: Linear optical properties of bimetallic ring resonator arrays.
(A) Schematic of a bimetallic metamaterial array. In the presence of an external magnetic field (represented by the green lines), the metamaterial induces rotation of the polarization azimuth angle, φ, on the incident beam. The inset is a scanning electron microscope (SEM) image of a fabricated sample. (B) Characteristic transmission spectra of a metamaterial sample with Ni sector that spans 90° illuminated with light polarized in the symmetry plane of the ring. Similar resonant behavior is observed for the orthogonal polarization (see Figure 1 of Supplementary Material). The dashed line is obtained by a computational analysis of an infinite 2D array, while the solid line corresponds to the experimentally measured spectra of a $100 \times 100\ \mu m^2$ metamaterial sample. Inset: Electric field distribution in the vicinity of the bimetallic ring at resonance ($\lambda = 850$ nm). (C) Transmittance of regular arrays consisting of bimetallic rings with Ni sector varying from 0° to 360°, calculated numerically. The three colored lines correspond to different fabricated samples (90° – red/III, 135° – green/II and 180° – blue/I).

electric dipole mode of the ring. Owing to the symmetry of the bimetallic ring resonators and the absence of splits, only symmetric current configurations can be excited by an incident wave, while anti-symmetric excitations commonly encountered in the context of Fano resonances are not allowed [20]. Scattering and dissipation in the bimetallic metamaterial system are determined by the regions of high current density. Strong currents in the Ni sector reduce the total power scattered at resonance, as nickel is less conductive and exhibits higher Joule losses than gold. In accordance, increasing the Ni sector size leads to damping of the resonance and to a decrease of its Q-factor, as can be deduced from Figure 1C. Such changes in the ring composition also alter the effective permittivity of the hybrid structure and shift the position of the resonance towards shorter wavelengths.

In the presence of an external magnetic field (H), the permittivity tensor of Ni becomes non-diagonal, which affects the polarization state of the light transmitted through the sample. The rotation of polarization azimuth induced by the magnetic field was experimentally measured, and the results are shown in Figure 2. For all three arc lengths of the Ni sector (90°, 135°, and 180°), the Faraday rotation spectra follow closely the linear optical response with the maxima of rotation occurring close to the plasmonic resonance frequency. Importantly, smaller Ni sectors lead to a stronger FE; reducing by 50% the arc length of the Ni sector (from 180° to 90°) leads to a 40% increase of peak rotation (from 0.29 mrad to 0.41 mrad). Simultaneously, the linewidth of the Faraday rotation resonance decreases significantly. These features are reproduced by finite element simulations (dashed curves) following a normalization of the numerical transmittance spectra to the experimental ones (described in the Materials and methods section). Moreover, in the numerically obtained Faraday spectra, the peak position experiences a relatively minor blue shift while varying the Nickel section angle from 90° to 180°. This is a direct result of changes in the effective permittivity of the ring. In the case of the experimental measurements, the Faraday maximum follows a non-monotonic dependence on the Ni sector arc length. We attribute this discrepancy to fabrication imperfections including inhomogeneities in the manufactured arrays and departures of the Ni sector from an ideal circular arc shape.

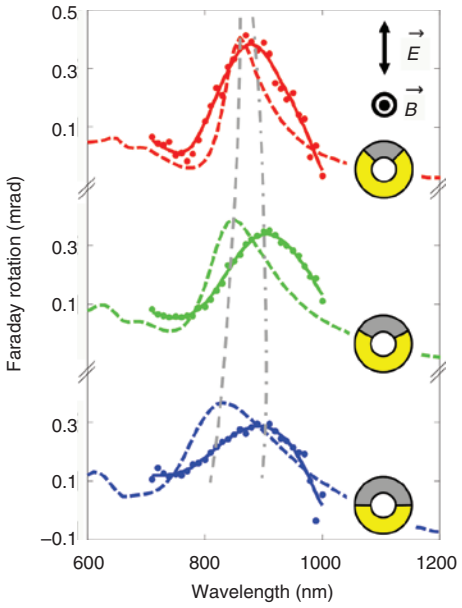

Figure 2: Faraday rotation of polarization azimuth.
Dots describe the experimental results for samples with Ni sectors that span over 90° (red), 135° (green), and 180° (blue) in the presence of a 100-mT external magnetic field. Solid lines act as guide for the eye. Dashed lines represent the corresponding computational results when transmission is normalized to the experimental values (see Materials and methods). The dashed grey line follows the peak position of simulation data, as seen in Figure 4A, while dot-dashed line shows the corresponding trend for the experimental results.

The counterintuitive dependence of the MO activity on the Ni sector arc length suggests that the Faraday rotation is controlled by resonant field enhancement in the vicinity of the Ni section. In particular, the incident electric field excites resonantly the Au part of the ring, which in turn induces currents in the Ni sector along the circumference of the arc. Owing to the off-diagonal elements of the Ni permittivity tensor in the presence of an external magnetic field, the induced currents in the Ni sector are coupled to radial charge oscillations resulting in a net component orthogonal to the polarization of the incident wave [21]. Hence, the bimetallic rings radiate fields polarized both parallel and orthogonal to the electric field of the incident wave leading to the observed Faraday rotation. In order to quantify the enhancement of Faraday rotation, we compare the MO response of the metamaterial to that of a continuous Ni film. As the latter exhibits negligible transmission, a straightforward comparison of the FE in these two systems is not instructive. Instead, as a figure of merit (FOM), we use the scattered electric field component, which is perpendicular to the incident polarization, normalized to the incident electric field and to the Ni filling factor. The FOM is calculated as $\mathrm{FOM} = \frac{|E_{sc}|\sin(\phi)}{|E_{inc}|f} \simeq \frac{|E_{sc}|\phi}{|E_{inc}|f}$ (in the small angle approximation), where ϕ is the Faraday rotation angle, f is the Ni filling factor, E_{sc} and E_{inc} are the amplitudes of the scattered and incident electric fields, respectively. This FOM allows for a comparison between the MO response of the

metamaterial in transmission and that of a continuous nickel film in reflection. Taking into account that the metamaterial sample with a 90° Ni sector has a peak rotation of ~0.41 mrad at 880 nm, transmittance of ~10%, and Ni filling factor of 6%, the resulting value of $FOM_{MM} \approx 2.16 \times 10^{-3}$. In comparison, a continuous 60-nm thick Ni film exhibits a reflectance of 70% and an MO rotation of 0.4 mrad at the same wavelength resulting in $FOM_{Ni} \approx 0.33 \times 10^{-3}$. Hence, the metamaterial leads to an enhancement of MO activity of $\frac{FOM_{MM}}{FOM_{Ni}} \simeq 6.5$. If we use the power of incident and scattered waves instead of the electric field amplitudes for calculating FOM, the enhancement reduces to ~2.55. Remarkably, at the resonance frequency, the metamaterial rotates the polarization of the incident wave equally to a nickel film of the same thickness but only with a nickel filling factor of 6%.

Owing to the anisotropic nature of the bimetallic rings, the MO response depends strongly on the polarization of the incident wave. The geometrical position and span of the two metal segments create a system with a single plane of symmetry, deviating from which affects both the plasmonic and MO response. In Figure 3B, we can see that the geometrical anisotropy of the sample leads to polarization conversion (in the absence of external static magnetic fields). Varying the angle of polarization azimuth of the excitation beam from 0° to 360° results in a four-lobe rosette with the points of zero conversion at 0°, 90°, 180°, and 270°. These points correspond to the polarization eigenstates of the system. In contrast, the effect of anisotropy becomes maximum at $n \times 45°$ (for $n = 1, 3, 5, 7$), and it results in a rotation of the incident polarization state by about 100 mrad. The introduction of an external magnetic field creates an additional contribution to the polarization rotation due to magnetically induced anisotropy, which leads to an offset of the total rotation. For opposite directions of magnetic fields, this effect appears as a splitting of the rotation curve, where the separation between the two curves corresponds to the Faraday rotation (see Figure 3A). The angle of the incident polarization azimuth shifts the current distribution along the ring (across areas of different dielectric properties), which significantly affects the plasmonic enhancement of the Faraday rotation. For angles of incident polarization that drives currents through more lossy areas (Nickel), the plasmonic resonance is damped and, thus, the Faraday rotation is reduced by almost 50% (Figure 3C). Here, we attribute the departure of the experimental curve from the theoretical one to small shifts of the beam within the sample in combination with the structural inhomogeneities in the metamaterial arrays.

A detailed numerical study of the effects of the ring composition and the incidence wave polarization on

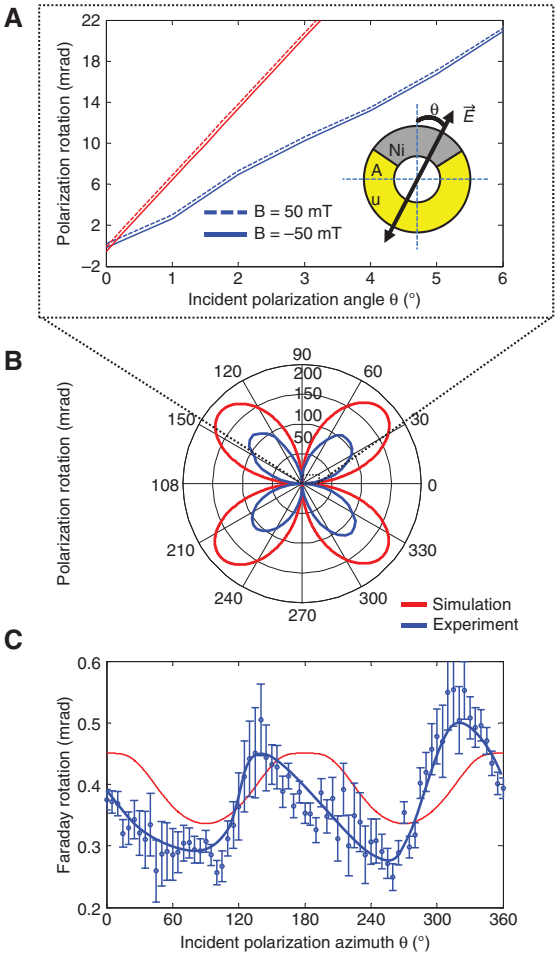

Figure 3: Sample optical anisotropy.
(A–B) Rotation of the polarization azimuth of a beam transmitted through the sample (135° Ni sector). Red lines represent computational analysis, and blue lines stand for experimental results. Solid and dashed lines represent opposite directions of external magnetic fields. θ is the angle of polarization azimuth in reference to the symmetry axis of the metamaterial array. (C) The effect due to the presence of the external magnetic field appears as the difference between the solid and dashed lines plotted in (A) and (B). The red line corresponds to numerical results, while blue circles represent experimental measurements. The blue line is a guide for the eye.

the Faraday rotation is presented in Figure 4A and B, respectively. In accordance to the experimental results of Figure 2, Figure 4A shows that the size of the nickel sector strongly impacts the Faraday rotation. Indeed, increasing the size of the Ni sector leads to an increase both in the dissipation loss (hence, a decrease in plasmonic field enhancement) and in the filling factor of the MO active material. These two competing mechanisms result in an optimum ring composition with an Ni sector of ~50°, away from which Faraday rotation rapidly decreases. Moreover, rings with Ni sectors smaller than 180° are highly sensitive

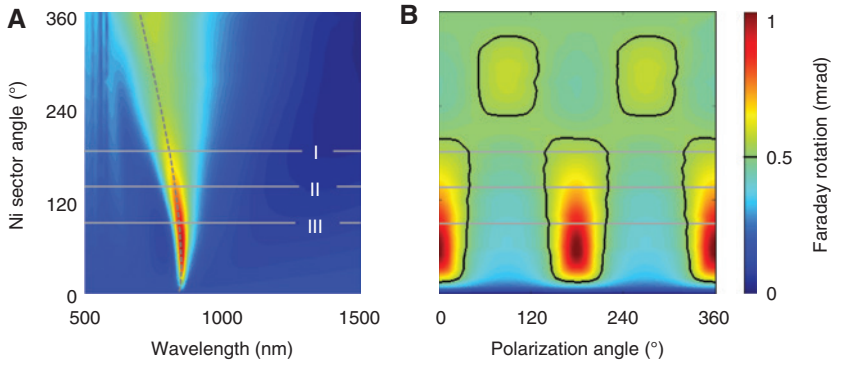

Figure 4: Bimetallic ring composition study.
(A) Faraday rotation spectra calculated for different ring compositions. (B) At resonance, denoted with dashed line on (A), Faraday rotation is calculated for different polarization angles of the incident beam, and an external static magnetic field of 100 mT.

to the polarization of the incident wave (see Figure 4B). For polarization along the *y*-axis (see inset to Figure 1A), the resonant currents flow mainly in the Au sector, which leads to a strong plasmonic resonance and (through field enhancement) to a high value of the Faraday rotation. When the polarization is rotated by 90°, the current density in Ni increases, which damps the MO response. On the contrary, for rings with large Ni sectors, the situation reverses and polarization angles normal to the symmetry plane of the ring offer a stronger MO response. In this case, due to the weaker plasmonic resonances, the modulation depth is reduced.

The dependence of the metamaterial MO response on the strength of the external magnetic field was investigated by hysteresis measurements, where the magnetic field intensity was varied while its orientation was maintained. The measurements reveal an almost linear magnetic field dependence and zero coercivity (Figure 5). These observations are explained by considering that the magnetic field is oriented normal to the plane of the nano-rings and that the field strength used in the experiment is not sufficient to saturate their magnetization. This behavior is strongly supported by the micromagnetic simulations, represented by the solid lines in Figure 5. The (numerically calculated) magnetization is connected by a linear relation to the (experimentally measured) Faraday rotation allowing, thus, for a direct comparison.

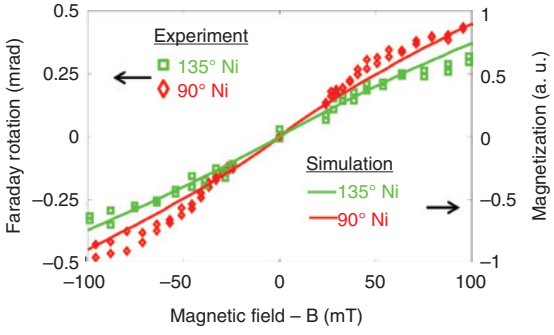

Figure 5: Hysteresis in bimetallic ring resonators.
Simulated (solid lines) and experimentally measured (markers) hysteresis in bimetallic rings with 90° (red) and 135° (green) Ni sector. Simulated data correspond to the magnetization of the system, while experimental results are presented in the form of Faraday rotation, which is proportional to the former.

3 Conclusion

We have introduced bimetallic nano-ring resonators as compact building blocks for MO devices. In particular, we have demonstrated experimentally multi-fold enhancement of the Faraday rotation in metamaterial arrays of such resonators where a nickel (surface) filling factor of 6% is sufficient to achieve the same MO effect as a continuous film of nickel. We also studied the dependence of the effect on external static magnetic fields, polarization of the incident wave, and wavelength as means of controlling the MO response of the metamaterial. We expect bimetallic metamaterials to find applications in refractive index and magnetic field sensing, as well as in compact active components for integrated nanophotonic circuits. In addition, this design has been shown to support transient thermoelectric currents that give rise to magnetic pulses [18, 19].

4 Materials and methods

4.1 Fabrication

The materials of choice for the bimetallic metamaterial system are Au and Ni, which comprise two arc sectors that

form a complete ring (Figure 1A). The angle, over which the Ni sector spans, controls the composition of the ring. Three samples have been fabricated on a glass substrate by electron-beam lithography with Ni sectors of 90°, 135°, and 180°. The mean diameter of the rings is 185 ± 5 nm with a linewidth of 65 nm and a height of 60 nm. Each sample comprises a regular array of 250 × 250 unit cells, positioned with a period of 400 nm and covering a total area of 100 × 100 μm^2. The fabrication process is separated in two steps, one for each of the two metals. In each step, metals are thermally evaporated on the substrate with a thickness of 60 nm and subsequently lifted off to reveal the design. A 50-nm-thick layer of co-polymer deposited underneath 200 nm of PMMA accelerates the lift-off process. The Ni part is deposited after Au to minimize any oxidization in the junctions between the two metals. Here, careful design and alignment are crucial in order to achieve good contact at the junctions. Discrepancies between the designed and fabricated samples can be attributed to the surface roughness, which is identified mainly in the Ni sector and has an RMS value that varies from 5 to 20 nm between individual unit cells. As Ni tends to form large grains, nanostructures suffer from small deformations, especially in the z-direction, due to the constrains that the e-beam lithography mask enforces in the x-y plane. Nevertheless, such deformations do not alter the plasmonic properties in a significant way as the latter mostly depends on the resonator dimensions in the plane perpendicular to light propagation (x-y plane). Furthermore, these artefacts are inconsistent across each sample and thus lead only to a small inhomogeneous broadening of the plasmonic resonances. Finally, we would like to note that the response of the bimetallic ring metamaterials does not depend strongly on the thickness of the metallic film. An increase of thickness would result in a minor enhancement of the magnetoplasmonic response due to an increase in resonance strength of the Au sections and changes in the magnetic shape anisotropy of the Ni sections [22].

4.2 Experimental characterization

The characterization of the linear optical properties in the vis-NIR for the fabricated samples was performed using a commercial microspectrometer (CRAIC Technologies Inc., San Dimas, CA, USA). A sensitive polarimeter setup, described in Ref. [23], was used in order to probe angles of polarization rotation with a precision of 10^{-5} mrad. The setup consists of a polarization modulator (Faraday modulator) positioned between two crossed polarizers. The sample is placed between the Faraday modulator and the second polarizer. The rotation can be derived by simultaneous detection locked in both the fundamental frequency and second harmonic of the modulator. For incident laser power P_s, the detected signal can be described by the following equation:

$$P_{out} = \frac{P_s}{2}(-4A\varphi cos(\omega t + \psi) + A^2 cos(2\omega t + 2\psi) + A^2), \quad (1)$$

where A is the rotation induced from the Faraday modulator, ω is its fundamental frequency, ψ is the arbitrary phase of the modulation, and φ is the polarization angle rotation we want to probe.

The two frequency components (fundamental frequency F and 2nd harmonic S signal) are recorded by lock-in detection. The rotation is derived as follows:

$$\varphi = -\frac{F}{S}\frac{A}{4}. \quad (2)$$

The rotation spectrum was measured by using a tunable laser source (Mai Tai from Spectra-Physics, Santa Clara, CA, USA) and a photo-detector. The wavelength of the source was varied between 700 and 1000 nm, with a step of 10 nm. The external magnetic field was provided by ring-shaped neodymium magnets placed in the propagation direction, in such a way as to form a magnetic field with direction normal to the sample plane. In order to accommodate hysteresis measurements in the setup, the distance between the magnets and the sample was varied in controlled steps.

4.3 Numerical simulations

The plasmonic and MO properties of the bimetallic metamaterials were simulated using the finite element method implemented in a commercial solver (COMSOL Inc., Burlington, MA USA). An infinite 2D array of resonators is assumed to be positioned on a semi-infinite glass substrate. In the presence of external magnetic fields, the permittivity tensor of Ni becomes non-diagonal [24–26]. Limiting the magnetic field vector to a direction normal to the plane of the sample reduces the off-diagonal elements to only a single non-zero pair:

$$\epsilon = \epsilon_r \begin{pmatrix} 1 & -i\beta & 0 \\ i\beta & 1 & 0 \\ 0 & 0 & 1 \end{pmatrix}, \quad (3)$$

where ϵ_r is the (isotropic) complex relative permittivity of the magneto-optically active material and β is a

frequency- and magnetic field-dependent MO parameter, obtained by interpolating values found in the literature [24, 27].

The Faraday effect depends strongly on the transmission of the medium, and even small differences between the experimentally and numerically obtained transmittance can lead to large discrepancies in the estimation of FE. In order to account for such effects, we normalize the amplitude of the calculated transmitted electric fields to the value we measure experimentally.

Hysteresis cycles of bimetallic nano-rings were simulated using OOMMF [28]. Additional magnetic parameters used are those commonly found in the literature for Ni [29], the magnetization saturation is 0.47 pJ/m, and the exchange constant is 8.2 pJ/m. The maximum applied external field H_z is 100 mT, and it is oriented perpendicular to the plane of the sample. The mesh size was $4\times4\times4$ nm^3, thus allowing accurate simulations while keeping reasonable computational times. The results presented in Figure 5 show a typical hysteresis curve for soft, thick magnetic films (where perpendicular magnetic anisotropy is not present), although modulated due to the non-extended geometry of the Ni sectors.

Acknowledgments: The authors would like to thank Anibal L. Gonzalez Oyarce for his advice on micromagnetic simulations and F. Javier Garcia de Abajo for numerous fruitful discussions. The authors acknowledge the support of the MOE Singapore (grant MOE2011-T3-1-005), the UK's Engineering and Physical Sciences Research Council (grants EP/G060363/1, EP/M008797/1), and the Leverhulme Trust. The data from this paper can be obtained from the University of Southampton ePrints research repository: http://dx.doi.org/10.5258/SOTON/405057.

References

[1] Zvezdin AK, Kotov VA. Modern magnetooptics and magnetooptical materials. CRC Press, New York, 1997.
[2] Safarov VI, Kosobukin VA, Hermann C, Lampel G, Peretti J, Marlière C. Magneto-optical effects enhanced by surface plasmons in metallic multilayer films. Phys Rev Lett 1994;73:3584–7.
[3] González-Daz JB, Garca-Martn A, Garca-Martn JM, et al. Plasmonic Au/Co/Au nanosandwiches with enhanced magneto-optical activity. Small 2008;4:202–5.
[4] Grunin AA, Zhdanov AG, Ezhov AA, Ganshina EA, Fedyanin AA. Surface-plasmon-induced enhancement of magneto-optical kerr effect in all-nickel subwavelength nanogratings. App Phys Lett 2011;97:261908.
[5] Wang L, Clavero C, Huba Z, et al. Plasmonics and enhanced magneto-optics in core-shell Co-Ag nanoparticles. Nano Lett 2011;11:1237–40.
[6] Chin JY, Steinle T, Wehlus T, et al. Nonreciprocal plasmonics enables giant enhancement of thin-film Faraday rotation. Nat Comm 2013;4:1599.
[7] Du GX, Mori T, Saito S, Takahashi M. Shape-enhanced magneto-optical activity: degree of freedom for active plasmonics. Phys Rev B Condensed Matter Mater Phys 2010;82:1–4.
[8] Feil H, Haas C. Magneto-optical kerr effect, enhanced by the plasma resonance of charge carriers. Phys Rev Lett 1987;58:65–8.
[9] Reim W, Weller D. Kerr rotation enhancement in metallic bilayer thin films for magneto-optical recording. App Phys Lett 1988;53:2453–4.
[10] Ferré J, Penissard G, Marliere C, Renard D, Beauvillain P, Renard JP. Magneto-optical studies of Co/Au ultrathin metallic films. App Phys Lett 1990;56:1588.
[11] Maccaferri N, Bergamini L, Pancaldi M, et al. Anisotropic nanoantenna-based magnetoplasmonic crystals for highly enhanced and tunable magneto-optical activity. Nano Lett 2016;16:2533–42.
[12] Belotelov VI, Akimov IA, Pohl M, et al. Enhanced magneto-optical effects in magnetoplasmonic crystals. Nat Nanotechnology 2011;6:370–6.
[13] Maccaferri N, Gregorczyk KE, de Oliveira TVAG, et al. Ultrasensitive and label-free molecular-level detection enabled by light phase control in magnetoplasmonic nanoantennas. Nat Comm 2015;6:6150.
[14] Kataja M, Pourjamal S, Maccaferri N, et al. Hybrid plasmonic lattices with tunable magneto-optical activity. Opt Express 2016;24:3652.
[15] Chau KJ, Irvine SE, Elezzabi AY. A gigahertz surface magneto-plasmon optical modulator. Quantum Elec IEEE 2004;40:571–9.
[16] Sepúlveda B, Calle A, Lechuga LM, Armelles G. Highly sensitive detection of biomolecules with the magneto-optic surface-plasmon-resonance sensor. Opt Lett 2006;31:1085–7.
[17] Zubritskaya I, Lodewijks K, Maccaferri N, et al. Active magneto-plasmonic ruler. Nano Lett 2015;15:3204–11.
[18] Tsiatmas A, Atmatzakis E, Papasimakis N, et al. Optical generation of intense ultrashort magnetic pulses at the nanoscale. New J Phys 2013;15:113035.
[19] Vienne G, Chen X, Teh YS, Ng YJ, Chia NO, Ooi CP. Novel layout of a bi-metallic nanoring for magnetic field pulse generation from light. New J Phys 2015;17:013049.
[20] Fedotov VA, Rose M, Prosvirnin SL, Papasimakis N, Zheludev NI. Sharp trapped-mode resonances in planar metamaterials with a broken structural symmetry. Phys Rev Lett 2007;99:147401.
[21] Maccaferri N, Berger A, Bonetti S, et al. Tuning the magneto-optical response of nanosize ferromagnetic Ni disk using the phase of localized plasmons. Phys Rev Lett 2013;111:167401.
[22] Atmatzakis E, Papasimakis N, Zheludev NI. Plasmonic absorption properties of bimetallic metamaterials. Microelectron. Eng. 2017;172:30–4.
[23] Bennett PJ. Novel polarization phenomena and their spectroscopic application in bulk solids and films. PhD thesis, University of Southampton, 1998.
[24] Goto T, Hasegawa M, Nishinomiya T, Nakagawa Y. Temperature dependence of magneto-optical effects in nickel thin films. J Phys Soc Jap 1977;43:494–8.

[25] Argyres PN. Theory of the Faraday and Kerr effects in ferromagnetics. Phys Rev 1955;97:334–45.
[26] Zharov AA, Kurin VV. Giant resonant magneto-optic Kerr effect in nanostructured ferromagnetic metamaterials. J App Phys 2007;102:123514.
[27] Snow C. The magneto-optical parameters of iron and nickel. Phys Rev 1913;2:29–38.
[28] Porter DG, Donahue MJ. Oommf user's guide, version 1.0, interagency report nistir 6376, 1999.
[29] Talagala P, Fodor PS, Haddad D, et al. Determination of magnetic exchange stiffness and surface anisotropy constants in epitaxial $ni_{1-x}co_x$(001) films. Phys Rev B 2002;66:144426.

Supplemental Material: The online version of this article (DOI: 10.1515/nanoph-2016-0162) offers supplementary material, available to authorized users.